Conference on Modelling Fluid Flow (CMFF'25)
The 19th International Conference on Fluid Flow Technologies
Budapest, Hungary, August 26 - August 29, 2025

LASER-OPTICAL VALIDATION AND COMPARATIVE ANALYSIS OF NUMERICAL HEAT TRANSFER MODELS FOR SINGLE NOZZLE IMPINGEMENT FLOWS

Eileen Trampe[1], Jan-Henrik Rieger[2], Dominik Büschgens[3], Christian Wuppermann[4]

[1] Corresponding Author. Department for Industrial Furnaces and Heat Engineering, RWTH Aachen University, 52074 Aachen, Germany. Tel.: +49-241-80-26051, E-mail: trampe@iob.rwth-aachen.de
[2] Department for Industrial Furnaces and Heat Engineering, RWTH Aachen University, 52074 Aachen, Germany. E-mail: jan-henrik.rieger@rwth-aachen.de
3 Department for Industrial Furnaces and Heat Engineering, RWTH Aachen University, 52074 Aachen, Germany. E-mail: bueschgens@iob.rwth-aachen.de
4 Department for Industrial Furnaces and Heat Engineering, RWTH Aachen University, 52074 Aachen, Germany. E-mail: wuppermann@iob.rwth-aachen.de

ABSTRACT

A wide variety of heating and cooling applications, including thermal processing, use impingement nozzles for their high heat-transfer coefficients. The resulting thermal loads still require large volume flows and thus process-scale nozzle diameters, resulting in Reynolds numbers of $Re \approx 1 \times 10^4 - 1 \times 10^5$. This work presents a combined thermal- and fluid-dynamic investigation of impingement jets from a single round and a single slot nozzle under these conditions. A central focus is the systematic comparison of the three turbulence models SST *k-ω*, generalized *k-ω* (GEKO) and Reynolds Stress Model (RSM) to identify the option that delivers the most accurate simulation of industrial impingement jets. The validation of the numerical results is based on the experimentally determined heat transfer at a strip and laser-optical Particle Image Velocimetry (PIV) measurements. An optimised set of GEKO parameters further reduces heat-transfer error. The strengths and shortcomings of each model in predicting local velocity, turbulent kinetic energy and heat transfer are revealed by the PIV data.

Keywords:
Computational Fluid Dynamics, Convective Heat Transfer, Impingement Jets, Particle Image Velocimetry, Turbulence Models

NOMENCLATURE

C_{CUR}	[-]	curvature Parameter
C_{MIX}	[-]	mixing Parameter
C_{NW}	[-]	near Wall Parameter
C_{SEP}	[-]	separation Parameter
D	[*mm*]	nozzle diameter
D_h	[*mm*]	hydraulic diameter
H	[*mm*]	strip distance
k	[m^2/s^2]	turbulent kinetic energy (TKE)
μ	[$Pa \cdot s$]	dynamic viscosity
Nu	[-]	Nusselt number
p	[Pa]	pressure
ρ	[kg/m^3]	fluid density
Re	[-]	Reynolds number
SRN	[-]	single round nozzle
SSN	[-]	single slot nozzle
u	[m/s]	fluid velocity
t	[*mm*]	thickness
W	[*mm*]	nozzle width
Φ	[W/m^3]	heat generation
ω	[s^{-1}]	specific turbulence dissipation rate

1. INTRODUCTION

Impingement jets are used in a variety of heating and cooling applications, including thermal processing. Typically, round or slot nozzles are used for the heat treatment of metal strips [1,2]. The first design of these nozzle systems is carried out using empirically derived Nusselt relations, a detailed and sophisticated design makes complex experimental measurements unavoidable [3,4]. Numerical simulation is intended to shorten this development process for new nozzle systems and reduces the number of nozzle system prototypes. However, to this day the prediction accuracy is still insufficient, which is one of the hurdles why numerical modelling is not widely used in industry [5].

The numerical modelling of impingement jets poses a significant challenge due to the substantial variations in flow characteristics along the flow

direction. The flow emerges from the nozzle exit as a free jet, and given the prevailing technical conditions, a turbulent flow structure can be predicted [6]. The subsequent spreading and deceleration of the free jet are a consequence of its interaction with the ambient medium through mixing and momentum exchange. As the distance to the wall surface increases, the free jet transitions into a stagnation point flow, whereby the flow is deflected by the wall. This stagnation zone is characterised by increased turbulence. The subsequent wall jet exhibits flow structures analogous to those of the free jet, widening as the flow velocity increases, while the mean flow velocity decreases. [3,7]

The study aims to investigate whether RANS-based turbulence modelling can predict the flow and heat transfer of industrial-scale impingement nozzles with an accuracy of 5 %, which is required for nozzle-system design. Compared to numerical studies in other application areas, this is an ambitious goal [5,8–11]. In order to expose the limitations of the models and establish a realistic error bound, the simulations are benchmarked against an extensive, high-resolution PIV dataset that resolves the entire impingement region, as well as strip heat-flux measurements. In addition, the potential of the GEKO model, for which there is still little comparative data, is investigated. Optimised GEKO parameters are used for this purpose. The results will be thoroughly compared with data from other publications in the discussion.

2. Problem Description

For the study, a $W = 5$ mm single slot nozzle (SSN) and a $D = 25$ mm single round nozzle (SRN) were used, with a distance of $H = 50$ mm between the nozzle and the strip on which the impingement jet is directed. The test conditions are outlined in Table 1. The Reynolds number for this flow configuration is defined as (1) [7],

$$Re_x = \frac{u\rho x}{\mu} \tag{1}$$

The heat transfer of these nozzles has previously been the subject of an experimental study, thus resulting in the availability of data from these measurements for the purpose of validation. In the experiment, the heat transfer is determined by heating a constantan® strip while it is cooled by the flow. The temperature on the strip is recorded with an infrared camera. The local Nusselt number per pixel can be calculated from the temperature profile, as Trampe et al. [12] explain in their article.

Table 1. Test conditions

Geometry	H/D_h	u	Re
Slot	5	15.8 m/s	11,870
Slot	5	85.0 m/s	54,900
Round	2	19.3 m/s	33,250
Round	2	52.5 m/s	90,000

PIV measurements were conducted in advance to evaluate the simulated flows and quantify the resulting energy. The parameters measured include the flow velocity u and the turbulent kinetic energy (TKE) k, which is a measure of the energy of the vortex movements of a flow. The data was collected on the same test rig that had previously been used to determine the heat transfer. The configuration was expanded to encompass an Nd:YAG laser (wavelength 532 nm, Litron Lasers Ltd) and a camera (CX2-16, LaVision GmbH). The addition of di-ethyl-hexyl sebacate (DEHS) particles to the flow enabled the tracking of particle movement using LaVision's DaVis 11 software.

2.1 Physical modelling and Mesh

The present study investigates the convective heat transfer to a flat strip by an impinging jet, which is the basis of the 3D flow domain, Figure 1. The working medium is air, which is introduced into the flow domain through the nozzles (inlet). The fluid temperature and the fluid velocity are measured beforehand. The heated strip is modelled as a solid body with a thickness of $t = 0.1$ mm and subjected to a constant heat generation related to the experiment. The width of the strip corresponds to 60 times the nozzle width or 30 times the nozzle diameter. The sides of the fluid domain are defined as pressure outlets with a gauge pressure $p = 0$ Pa, while all other walls are assumed to be adiabatic. The fluid domain has a high level of agreement with Shukla's proposals [8].

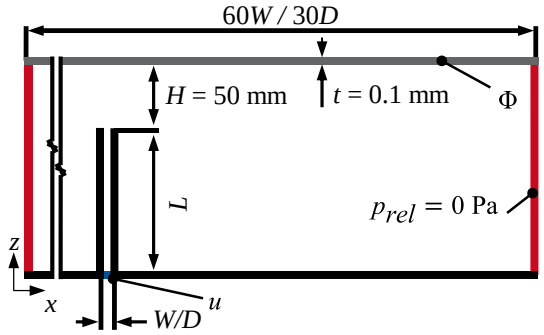

Figure 1. Sketch of the fluid domain for a single nozzle; black/grey: wall, blue: velocity inlet, red: pressure outlet.

In order to analyse the heat transfer on the constantan® strip and compare it with the measured data, a rake is placed over the constantan® strip. The number and spacing of the evaluation points of the rake correspond to the number of the pixels of the temperature measurement, therefore the evaluation points are spaced 1.28 mm apart.

A mesh dependence study was carried out with particular attention to the area near the constantan® strip. The dimensionless wall distance y^+ in this zone must be $y^+ \approx 1$ for high prediction accuracy [13,14]. The grid dependence study was carried out using the

generalized k-ω turbulence model with a nozzle exit velocity of u = 51.2 m/s for a SSN. This corresponds to the average Reynolds number of the studies conducted in this study. The key findings of the mesh dependency study are presented in Table 2.

Table 2. Key figures mesh dependency

Mesh	Cells	y^+_{min}	y^+_{ave}	$\overline{Nu}$	Nu_{Stag}
Coarse	4.3 Mio.	0.9	1.4	446	172
Medium	7.6 Mio.	0.7	1.1	441	171
Fine	15.3 Mio.	0.4	0.7	447	168

It was found that a stable solution was obtained with a mesh of 7.6 million cells. No further improvement was obtained by increasing the number of elements in the mesh. The medium mesh size of 7.6 million cells was selected for further investigation due to it offering the best compromise between computational time and Nusselt number prediction. When analysing the SRN, the same mesh properties are used.

2.2 Turbulence Modelling

A pre-selection of turbulence models was based on previous Reynolds-Averaged Navier-Stokes (RANS) simulations [5], with the k-ω (Shear Stress Transport) SST and generalized k-ω turbulence (GEKO) models chosen due to their low computational cost and good agreement for simulating impingement jets. The k-ω SST model is based on the k-ω standard model in the boundary layer region, and this two-equation model solves one transport equation, each for the TKE k (2) and the vortex frequency ω (3). In these equations, $G_{k,\omega}$ denotes the production of k and ω, respectively. $\Gamma_{k,\omega}$ represents the effective diffusion of k and w, while $Y_{k,\omega}$ represents the dissipation due to turbulence. The generation of turbulence due to the buoyancy effect is denoted by $G_{k,\omega.}$ The source terms, $S_{k,\omega}$, are user-defined.

$$\frac{\partial}{\partial t}(\rho k) + \frac{\partial}{\partial x_i}(\rho k u_i) = \frac{\partial}{\partial x_j}\left(\Gamma_k \frac{\partial k}{\partial x_j}\right) + G_k - Y_k + S_k + G_b \quad (2)$$

$$\frac{\partial}{\partial t}(\rho \omega) + \frac{\partial}{\partial x_i}(\rho \omega u_i) = \frac{\partial}{\partial x_j}\left(\Gamma_\omega \frac{\partial \omega}{\partial x_j}\right) + G_\omega - Y_\omega + S_\omega + G_{\omega b} \quad (3)$$

In the free jet region, the k-ω SST model behaves like the k-ε model, showing good convergence rates. The integration of the standard k-ω and k-ε models offers the benefit of enabling the modelling of both the near wall region and the free jet region in a meaningful manner. The GEKO turbulence model is also founded on the two equations of the k-ω model, but it possesses six additional independent parameters that can be adjusted without compromising the fundamental tenets of the model [15].

The Reynolds Stress Model (RSM) was selected as the third turbulence model. In contrast to the preceding turbulence models, the RSM characterises each respective Reynolds stress using a single equation. This approach abandons the conventional assumption of isotropic turbulence, but also involves a higher computational cost. The RSM stress-ω with shear flow correction was applied in the present work. [16]

3. RESULTS AND DISCUSSION

In the following sections, the local Nusselt number distributions, velocity distributions and the distribution of turbulent kinetic energy are presented for the slot and round nozzle. In each case, a low Reynolds number and a high Reynolds number are analysed.

3.1 Study of various turbulence models

Figure 2 shows the averaged Nusselt number at a Reynolds number of Re = 11,870 above the relative position of a SSN. All turbulence models tend to calculate a lower Nusselt number in the stagnation point than the experimental PIV measurement. The deviation in the stagnation point is 5.5 – 12 %. From the relative position x/D_h = 2, the SST k-ω and GEKO Default model approach the experimental solution but remain below the measured course of the Nusselt number. The RSM delivers consistently lower Nusselt numbers with an average deviation of 36.3 %.

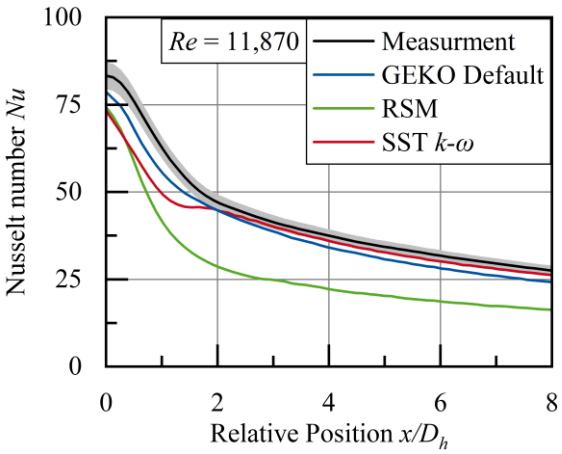

Figure 2. Distribution of *Nu* in cross-section for a SSN *W* = 5 mm, *Re* = 11,870

Figure 3 shows the flow distribution over the relative position x/D_h and the strip distance H. The PIV image corresponds to the experimental measurement. All turbulence models calculate a similar core velocity in the free jet, but a smaller shear layer compared to the PIV measurement. A developed stagnation zone is recognisable in each case. The SST k-ω and GEKO Default model show a local velocity maximum at $x/D_h \approx 1$ in the forming boundary layer zone. The RSM predicts significantly higher velocities in the wall jet than the measurement. The experimental PIV measurement shows a lower velocity and no local maxima.

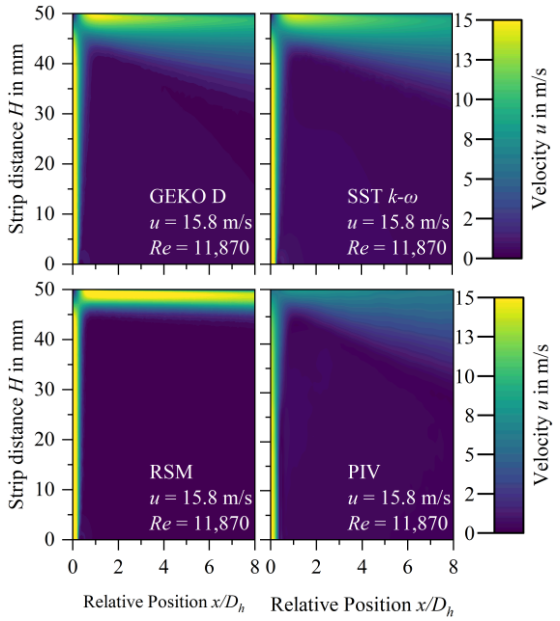

Figure 3. Velocity distribution for a SSN *W* = 5 mm, *Re* = 11,870

Figure 4 shows the turbulent kinetic energy k along the relative position x/D_h and strip distance H. The SST k-ω and GEKO Default model calculate high values of the TKE in the shear flows of the free jet and the wall flow. In contrast, the RSM shows hardly any significant distribution of k over the relative position x/D_h for a given Reynolds number of Re = 11,870.

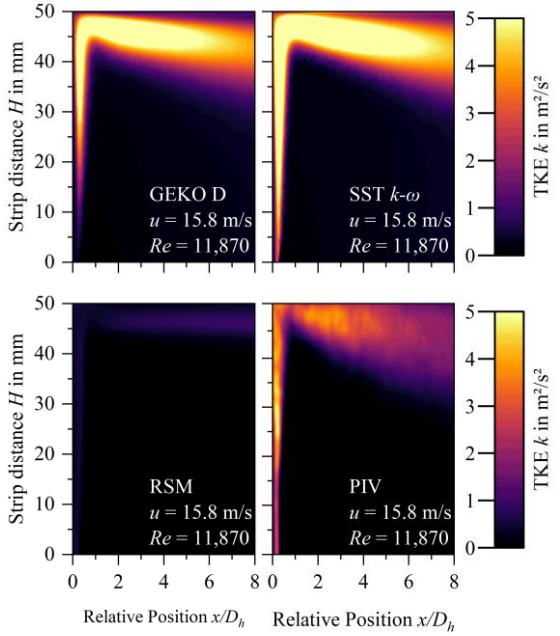

Figure 4. TKE distribution for a SSN *W* = 5 mm, *Re* = 11,870

For a higher flow velocity u = 85 m/s, the Reynolds number for the SSN is Re = 54,900. The corresponding local Nusselt numbers are shown in Figure 5. The experimental Nusselt number in the stagnation point increases by a factor of 2. The SST k-ω and GEKO Default models calculate a Nusselt number that is 9.6 % and 19.7 % higher at the stagnation point. In contrast, the RSM shows good agreement at the stagnation point, with a small deviation of 0.1 %. However, the RSM underestimates the Nusselt number over the full strip length, with an average deviation of 24.3 %.

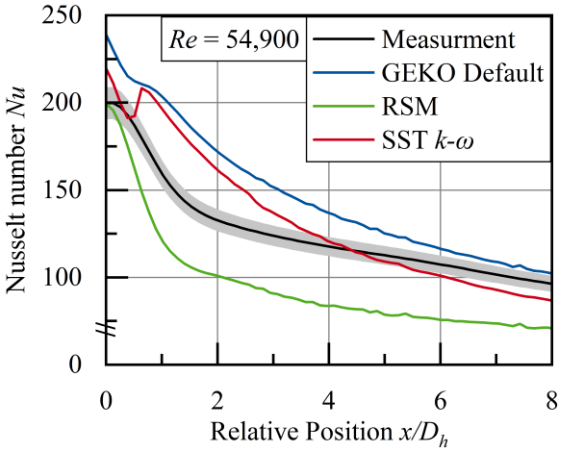

Figure 5. Distribution of *Nu* in cross-section for a SSN *W* = 5 mm, *Re* = 54,900

The SST k-ω model is the only model that calculates a secondary local peak at x/D_h = 1, which is not present in the PIV measurement. The SST k-ω model runs above the measurement up to $x/D_h \approx 4.5$ also intersecting the measurement curve. The GEKO Default model consistently calculates Nusselt numbers that are too high.

The velocity fields for u = 85 m/s of the SST k-ω and GEKO Default models, shown in Figure 6, are similar. A pronounced stagnation zone can be seen at x/D_h = 0, with a local velocity maximum building up due to the pressure gradient at x/D_h = 1. The wall jet widens further along the relative position.

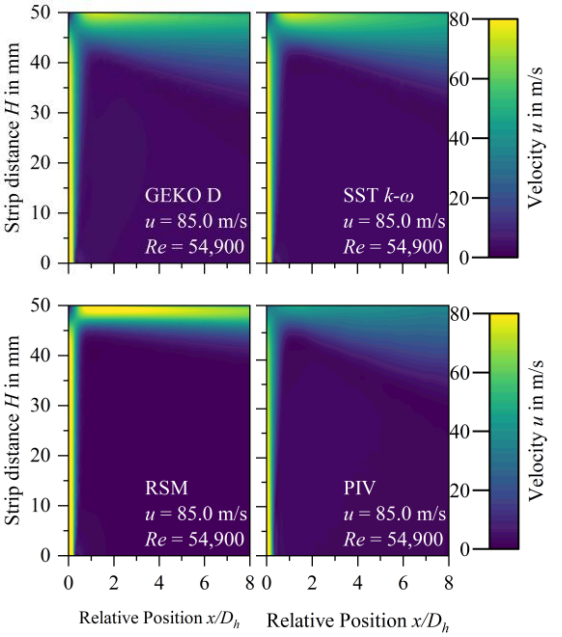

Figure 6. Velocity distribution for a SSN *W* = 5 mm, *Re* = 54,900

The velocity field of the RSM shows a smaller expansion of the wall jet, but a strongly pronounced local maximum and a subsequent high velocity within the wall jet. The PIV measurement shows a similar velocity distribution with a smaller local maximum at $x/D_h \approx 1$ and a larger jet expansion compared to the SST k-ω and GEKO Default results.

For the Reynolds number Re = 54,900 the TKE distribution along the impingement and the wall jet of the SSN is shown in Figure 7. For the SST k-ω and GEKO Default models, the distribution is similar to Figure 4, but with a significantly higher value of k. The RSM calculates significantly lower values compared to the other models and the PIV measurement. Compared to the PIV measurement, the SST k-ω and GEKO Default models calculate overall higher values for k.

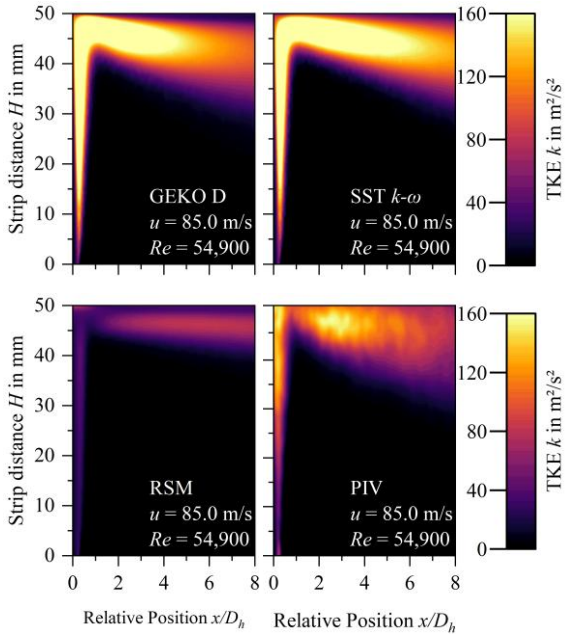

Figure 7. TKE distribution for a SSN W = 5 mm, Re = 54,900

Figure 8 shows the local Nusselt number over the relative position x/D_h of a SRN for a flow velocity at the nozzle outlet of u = 19.3 m/s. For the present boundary conditions this means a Reynolds number of Re = 33,250. All turbulence models calculate an excessive Nusselt number in the stagnation zone compared to the measurement. The local deviation of the turbulence models in the stagnation point is between 26.1 – 45.1 %. In addition, a deviating maximum of Nu is calculated at $x/D_h \approx 1$. This shift of the maximum away from the stagnation point was also observed in [17,18]. The SST k-ω model is closest to the experimental measurement and provides the second local Nu maximum correctly, which results in an average deviation of 24.7 %. The RSM and GEKO Default model have mean deviations of 5.9 % and 29.3 %, respectively, with the second local maximum not being well located. It is evident that the specification of a mean deviation may not always be meaningful, as the SST k-ω model reflects the local Nusselt number more accurately, yet exhibits a higher mean deviation.

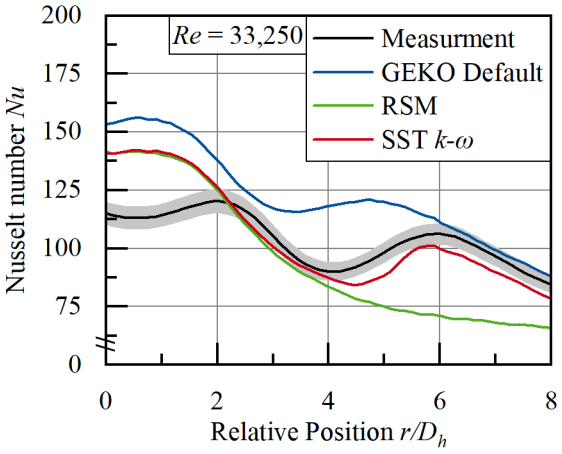

Figure 8. Distribution of Nu in cross-section for a SRN D = 25 mm, Re = 33,250

The velocity distribution of the measured and calculated flow velocity u for the SRN is shown in Figure 9. The turbulence models calculate a significantly larger shear layer of the free jet after the nozzle exit, while the PIV measurement shows a sharper boundary between the jet and the ambient air. All turbulence models show a pronounced stagnation zone as well as a forming and accelerating wall jet. Compared to the velocity profiles of the slot nozzles in Figure 3 and Figure 6, the wall jet of the RSM is in better agreement with the other models and the PIV measurement.

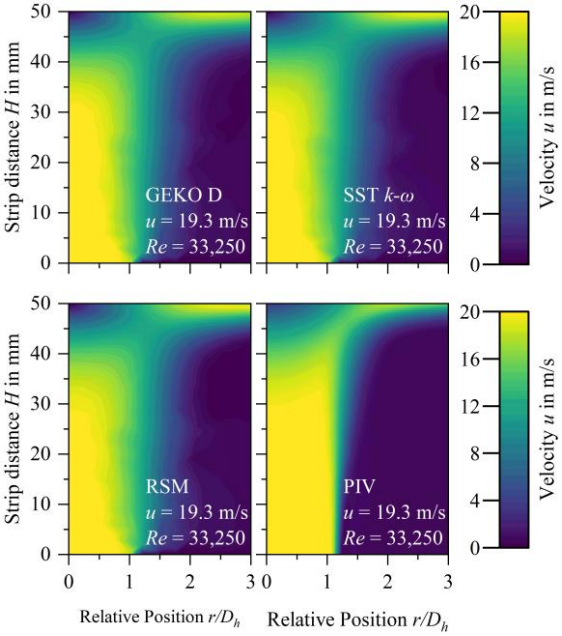

Figure 9. Velocity distribution for a SRN D = 25 mm, Re = 33,250

Figure 10 presents the TKE distribution for the SRN considered at Reynolds number Re = 33,250. As previously observed, the RSM calculates negligible levels of TKE $k \approx 1.5$ m²/s². There is no difference between the values in free jet or wall jet.

The GEKO Default and SST k-ω models calculate a higher k-values than the RSM. Consistent with the broad shear layers in Figure 9, a corresponding TKE distribution is shown over this range. The TKE distribution from the PIV measurement shows a strongly pronounced shear layer where the TKE reaches values up to twice as high as those calculated by the turbulence models.

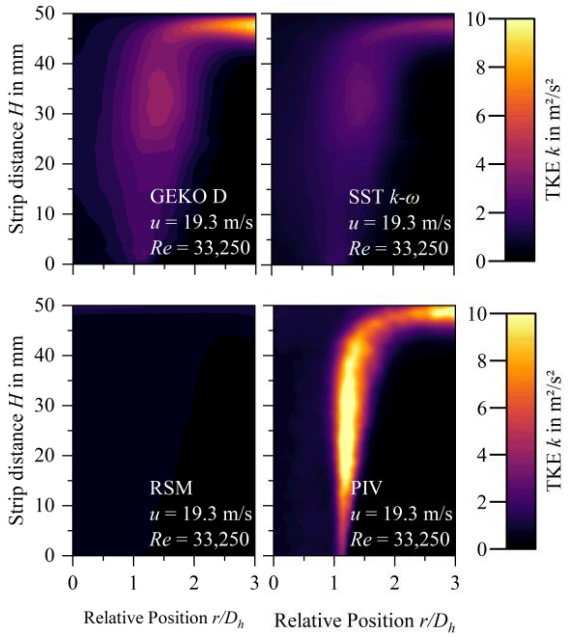

Figure 10. TKE distribution for a SRN D = 25 mm, Re = 33,250

Figure 11 shows the local Nusselt number Nu over the relative position x/D_h for a SRN with a flow velocity of u = 52.5 m/s. At this Reynolds number of Re = 90,000, all turbulence models calculate an excessive Nusselt number in the stagnation zone. The local deviation in the stagnation point is 23 – 33.3 %. It is noticeable that the RSM and GEKO Default model are close for the first local maximum in the range $0 \le x/D_h \le 2.5$. None of the models correctly predicts the second peak.

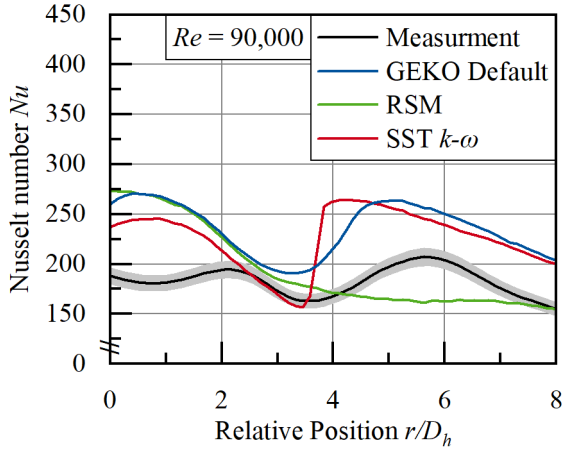

Figure 11. Distribution of Nu in cross-section for a SRN D = 25 mm, Re = 90,000

Figure 12 visualises the velocity distributions for the SRN. Despite the overall higher velocity level, the velocity curves are similar to those in Figure 9. The velocity distributions resulting from the numerical models again show a much more pronounced shear layer between the jet and its surroundings. The inner potential core is clearly visible. The course of the PIV measurement shows a sharp separation between the jet and its environment.

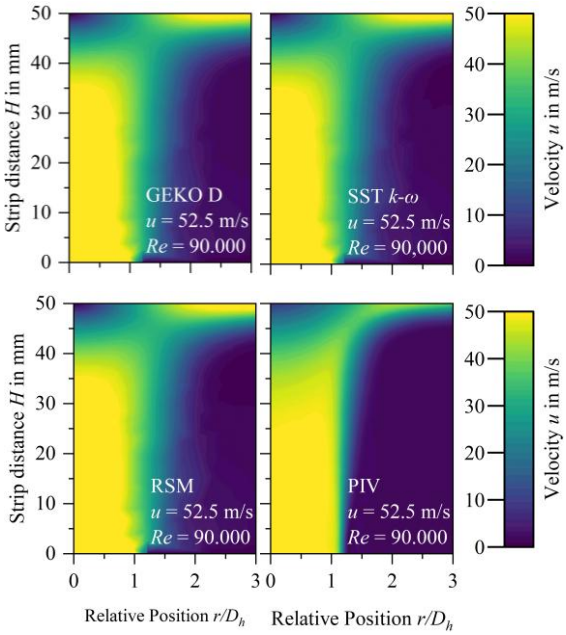

Figure 12. Velocity distribution for a SRN D = 25 mm, Re = 90,000

The TKE distributions for the SRN with Re = 90,000 are shown in Figure 13. The distribution is similar to those for the SRN with the lower flow velocity u in Figure 10, but the level of turbulent kinetic energy k is increased by a factor of 5.

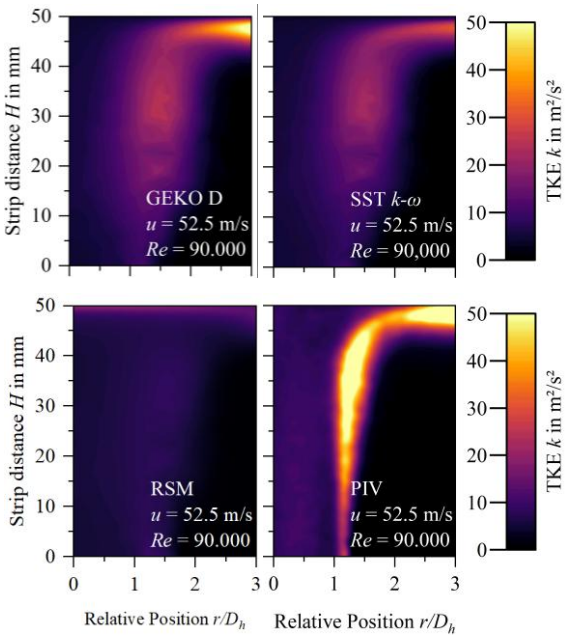

Figure 13. TKE distribution for a SRN D = 25 mm, Re = 90,000

The RSM again calculates very low values for k. In contrast, the GEKO Default and SST k-ω models produce a broader distribution of k with values at intermediate levels. The PIV measurement shows a well-defined shear layer in which the TKE reaches values up to twice as high as in the simulations.

3.2 GEKO parameter study

In the following, the results of the GEKO Default model presented in Section 3.1 are compared with the adjusted parameters of the GEKO model for the SST and SRN. The parameters were set using the method used in Menzler [19]. The algorithm optimises the parameters in such a way that the mean deviation of the Nusselt number is minimised.

The default parameters of the GEKO model and their value ranges, as well as the adjusted GEKO parameters, are shown in Table 3. C_{JET} and C_{CORNER} do not affect the local Nusselt number according to Menzler [19] and are therefore neglected.

Table 3. Investigated GEKO parameters in comparison with the default values

Case	C_{SEP}	C_{NW}	C_{MIX}	C_{CURV}
Default	1.75	0.50	0.30	1.00
Minimum	0.70	2.00	1.00	1.50
Maximum	2.50	0.50	0.30	1.00
SSN; Re = 11,870	4.73	2.98	1.38	1.00
SSN; Re = 58,100	1.75	7.76	21.09	1.00
SRN; Re = 33,250	1.16	-0.69	-1.26	0.03
SRN; Re = 90,000	1.34	-0.31	-0.62	0.85

Figure 14 shows the local Nusselt numbers of the SSN over the relative position for the GEKO default and adjusted parameters. The deviation in the stagnation zone increases with increasing Reynolds number.

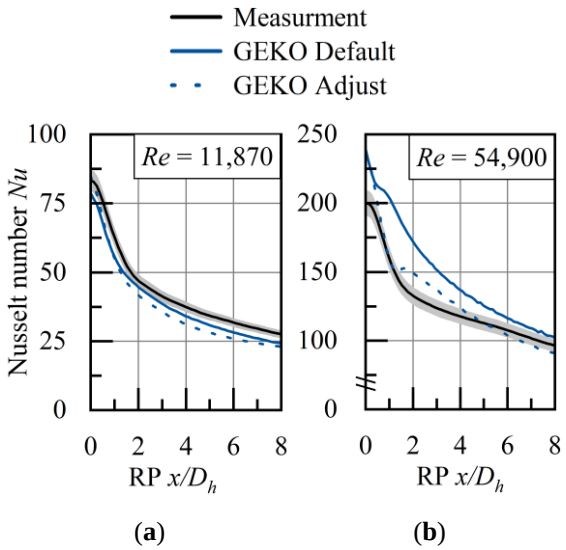

Figure 14. Distribution of *Nu* in cross-section for a SSN *W* = 5 mm (a) *Re* = 11,870 and (b) *Re* = 54,900

At a lower Reynolds number of Re = 11,870 the adjusted parameters lead to a similar deviation from the measurement than the default parameters as of a relative position of $x/D_h \approx 1$. At a higher Reynolds number of Re = 54,900, the adjusted parameters give a more accurate prediction with a mean deviation of only 1.6 %. However, the adjusted parameters lead to a local maximum at $x/D_h \approx 2$, which is not apparent from the measurement. After this local maximum, the Nu distribution runs above the measured values up to $x/D_h \approx 3$. The curve then intersects the measured values and runs below the experimental data, resulting in a smaller deviation on average.

Figure 15 presents the velocity distributions of the default and adjusted parameters for Re = 11,870 in the top two subfigures. The distributions show no qualitative difference. The bottom two subfigures show the TKE distribution. Again, there are no significant differences. This explains the similar Nusselt number curves in Figure 14.

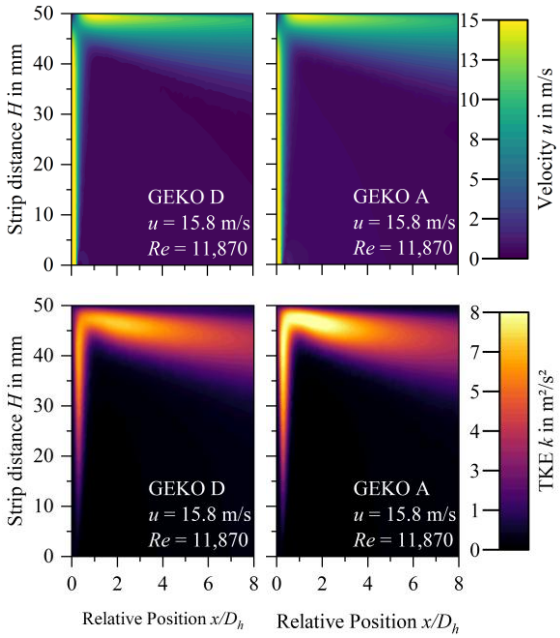

Figure 15. Velocity and TKE distribution for a SSN *W* = 5 mm, *Re* = 11,870

Figure 16 displays the velocity distributions for Re = 54,900 in the upper part of the figure, which are qualitatively similar. The lower part of the figure shows the TKE distribution, which, show significant differences. The adjusted parameters lead to an increased TKE range up to $x/D_h \approx 6$, while this range extends up to $x/D_h \approx 5$ for the default parameters.

Figure 17 shows the comparison of the GEKO default parameters and the adjusted parameters for the SRN. The lower Reynolds number Re = 33,250 and the higher Reynolds number Re = 90,000 are compared. For the lower Reynolds number Re = 33,250 both parameter sets lead to a significant local overestimation of Nu in the stagnation zone with a deviation of about 40 %. The maximum of the Nusselt number is shifted to the relative position $x/D_h \approx 1$. The adjusted parameters result in an

average deviation of *Nu* by 20.4 % compared to 30.3 % deviation for the default parameters.

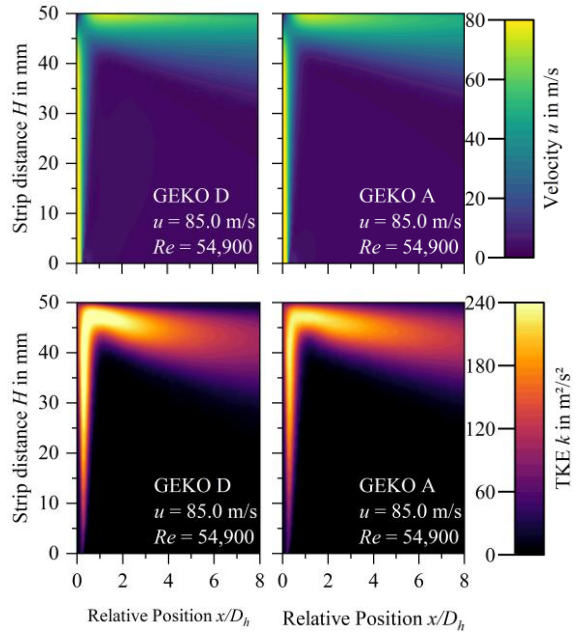

Figure 16. Velocity and TKE distribution for a SSN *W* = 5 mm, *Re* = 54,900

The position of the second local maximum is incorrectly predicted even with the adjust parameters. The local Nusselt numbers of *Re* = 90,000 show a qualitative agreement between measurement and simulation. But the absolute simulated values of *Nu* are significantly increased. The adjusted parameters shift the local minimum further to the measurement result and reduce *Nu* in the second local maximum. This results in an average deviation of 10 % compared to an average deviation of 16.0 % for the default parameters.

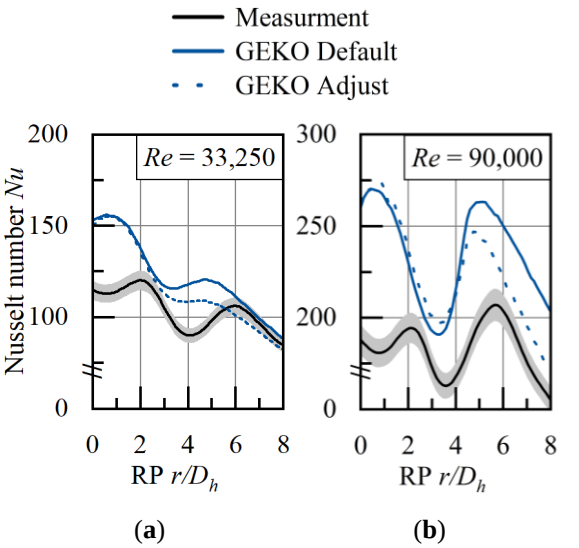

(a) **(b)**

Figure 17. Distribution of *Nu* in cross-section for a SRN *D* = 5 mm (a) *Re* = 33,250 and (b) *Re* = 90,000

Considering the lower Reynolds number of *Re* = 33,250, the velocity and TKE distributions of the default and adjusted parameters are plotted in Figure 18. The velocity distribution appears qualitatively similar. However, the TKE distribution show qualitative differences. With the default parameters, an increased TKE is calculated in the shear layer of the free jet, as well as a stronger local maximum at $x/D_h \approx 3$. With the adjusted parameters, an overall lower value for the TKE is calculated.

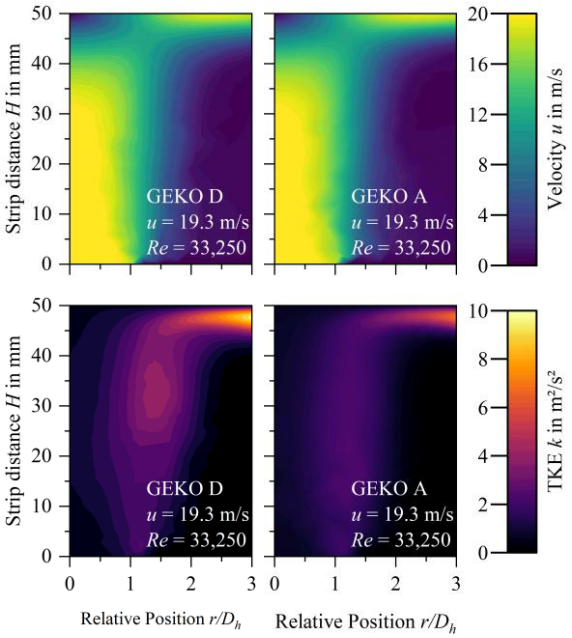

Figure 18. Velocity and TKE distribution for a SRN *D* = 25 mm, *Re* = 33,250

Figure 19 shows the velocity and TKE profiles of the SRN for *Re* = 90,000. The characteristics of the results show a high degree of agreement with the results shown in Figure 17 (SRN with *Re* = 33,250). Notably, these values are locally increased by a factor of 5 due to the increased nozzle exit velocity.

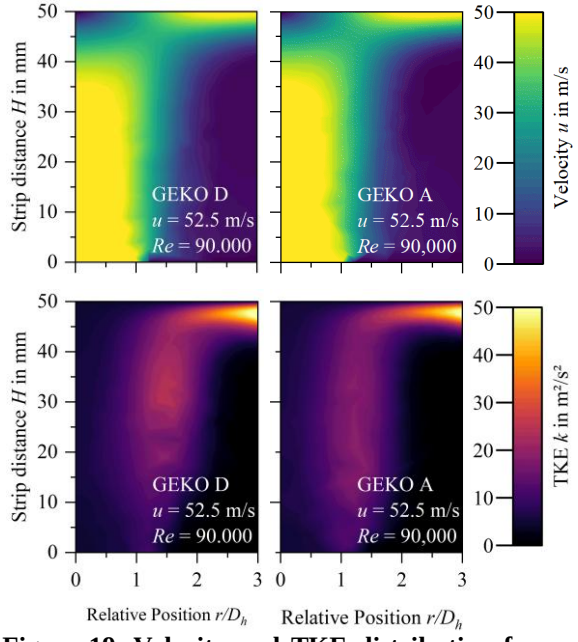

Figure 19. Velocity and TKE distribution for a SRN *D* = 25 mm, *Re* = 90,000

3.3 Discussion

In the following section, the results presented for the impingement jet modelling are discussed and the possible reasons for the insufficient prediction of heat transfer by the turbulence models are presented.

Figure 2 and Figure 5 show that the use of the RSM for the SSN application does not lead to a more accurate prediction of the Nusselt number as the two-equation models. There is no increase in accuracy for this application at the cost of more computation time. The TKE curves of the SSN in Figure 4 and Figure 6 show that the RSM underestimates the intensity of the turbulence, which could contribute to the lower Nusselt number shown in Figure 2 and Figure 5.

For the SRN application, the RSM also does not provide a significant improvement over the two-equation models, characterised by locally high deviations.

The present results of all cases indicate a proportional relationship between the TKE calculated by the turbulence models and the local Nusselt number. The calculated heat transfer rises with increasing TKE. However, the TKE is incorrectly reproduced locally, leading to over- and underestimation of the results. Therefore, it is necessary to adjust the TKE of the respective turbulence models in order to achieve a higher prediction accuracy. The velocities of the impingement jets are correctly represented using the numerical models and therefore do not lead to restrictions in the prediction accuracy.

The achieved prediction accuracy of the local Nusselt number is within the expected range [5]. Without a fundamental modification of the turbulence models, better predictions with RANS-based turbulence models do not seem to be possible. A further possibility is offered by the GEKO model, where the model parameters can be adapted to the specific application.

By optimising the GEKO parameters C_{SEP}, C_{NW}, C_{MIX} and C_{CURV}, an attempt was made to adapt the GEKO model to the considered impingement jets from single slot and round nozzles in order to increase the accuracy of the model. In some cases, values were obtained outside the recommended parameter ranges, the effects of which are not fully understood, see Table 3. For all applications considered, the average deviation for the result based on the adjust GEKO parameters was approximately halved. Even with the optimised parameters, there are still local deviations of up to 39.3 % in the stagnation zone and at the local maxima and minima. Yüksekdağ [17] and Rasheed [20] also optimised the GEKO parameters according to their research question. The investigations were carried out on SRNs with smaller diameters of D = 2.6 mm [17] and D = 15 mm [20] with a Reynolds number of Re = 23,000. Figure 20 compares the simulations carried out with the adjusted GEKO parameters according to Yüksekdağ and Rasheed and the results of this optimisation.

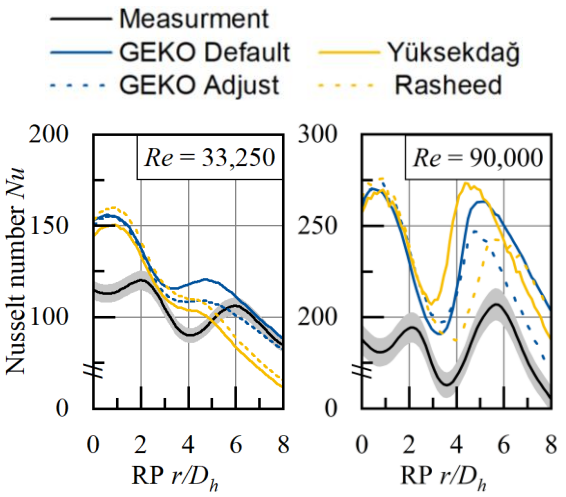

Figure 20. Distribution of *Nu* in cross-section for a SRN *D* = 5 mm (a) *Re* = 33,250 and (b) *Re* = 90,000 GEKO adjustments [17,20]

The comparison shows that the optimised GEKO parameters of Yüksekdağ and Rasheed achieve an improvement of the mean deviation for the SRN to Re = 33,250, but thus incorrectly reflect the local course. The GEKO parameters according to Yüksekdağ achieve a worse prediction accuracy for the SRN with Re = 90,000 than the default settings, while the GEKO parameters according to Rasheed are in the range of the optimisation of this study. This indicates that the optimised GEKO parameters are highly dependent on the geometry and flow conditions, i.e. the Reynolds number, and cannot be transferred without restriction.

Further optimisation potential would lie in a local optimisation of the GEKO parameters, e.g. the course of Nu in Figure 14 (b) could be locally influenced by the parameter C_{NW}. According to Menzler [19], the parameter C_{NW} has an influence on the gradient of Nu after the secondary peak, so that the curve could be further approximated to the experimental curve. Table 2 also shows that the adjusted GEKO parameters depend on the geometry (SSN/SRN) and the flow velocity respectively the Reynolds number. The GEKO model also offers the possibility of fine-tuning the parameters using sub-parameters, which should be investigated in a detailed parameter study.

4. SUMMARY

In this work, the local Nusselt number, velocity and turbulent kinetic energy distribution for impinging jets from single slot and round nozzles were investigated. In each case, a low and a high Reynolds number application have been compared. The main focus is on the comparison and suitability

of the turbulence models, the SST *k-ω* model, the GEKO model with default and adjust parameters and the RSM. The results of the numerical simulations were validated with experimental measurements carried out including heat transfer and PIV measurements. The discussion concluded that the RSM did not bring significant improvements in the prediction of the Nusselt number and underestimated the intensity of the turbulence, resulting in lower Nusselt numbers.

The SST *k-ω* and GEKO Default models performed as expected according to Zuckerman [5]. However, the prediction accuracy is far below the acceptable range for designing nozzle systems based on these simulations. Therefore, a further possibility to increase the prediction accuracy by optimising the GEKO parameters was investigated. The optimisation of the GEKO parameters showed improvements in the mean deviations and a strong dependence on the nozzle geometry respectively the Reynolds number.

For all models it was found that the turbulent kinetic energy is locally inaccurately predicted, while the flow velocities are accurately calculated. This leads to the conclusion that a fundamental modification of the model equations is necessary to increase the prediction accuracy of RANS-based turbulence models for the application of nozzle systems in thermo-process technology. Another possibility is to perform detailed parameter studies on optimised GEKO parameters. In an ideal scenario, superior GEKO parameters will be found that further reduce the discrepancies between simulation and experiment.

REFERENCES

[1] Kramer C, Hansen M, 2006, "Gas jet floatation for the touchless cooling of sensitive stainless steel strips in strip annealing lines", *Heat Processing* 24–26.

[2] Menzler D, 1992, "Konvektionskühlsysteme für Leichtmetallhalbzeuge", *Dissertation RWTH Aachen University, Aachen.*

[3] Martin H, 1977, "Heat and Mass Transfer between Impinging Gas Jets and Solid Surfaces", *Advances in Heat Transfer* Volume 13, Vol 13. Elsevier, pp 1–60.

[4] Hofmann HM,2005. "Wärmeübergang beim pulsierenden Prallstrahl", *Dissertation Universitätsverlag, Karlsruhe.*

[5] VDI e.V., 2013. *VDI-Wärmeatlas*, Springer Berlin Heidelberg, Berlin, Heidelberg.

[6] Bergman TL, Lavine AS, Incropera FP, Dewitt DP, 2011. *Fundamentals of Heat and Mass Transfer*, John Wiley & Sons.

[7] Zuckerman N, Lior N, 2006, "Jet Impingement Heat Transfer: Physics, Correlations, and Numerical Modeling", *Advances in Heat Transfer*, Vol 39. Elsevier, pp 565–631.

[8] Shukla A, Dewan A, 2017, "Flow and thermal characteristics of jet impingement: comprehensive review", *IJHT* 35:153–166.

[9] Barata B, Navalho J, Pereira J, 2023, "RANS simulations of plane impinging jets: On the influence of plate velocity in the Nusselt number secondary peak", *Therm* sci 27:4947–4960.

[10] Alimohammadi S, Murray DB, Persoons T, 2014, "Experimental Validation of a Computational Fluid Dynamics Methodology for Transitional Flow Heat Transfer Characteristics of a Steady Impinging Jet", *Journal of Heat Transfer* 136.

[11] Dutta R, Dewan A, Srinivasan B, 2013, "Comparison of various integration to wall (ITW) RANS models for predicting turbulent slot jet impingement heat transfer", *International Journal of Heat and Mass Transfer* 65:750–764.

[12] Trampe E, Rademacher N, Wulfmeier M, Büschgens D, Pfeifer H, 2024, "A High-Resolution Method for the Experimental Determination of the Heat Transfer Coefficients of Industrial Nozzle Systems in Heat Treatment Plants", *Applied Sciences* 14:3024.

[13] Cebeci, T, ed., 2013. *Analysis of turbulent flows with computer programs*, 3rd edn., Butterworth-Heinemann, Oxford.

[14] Kadivar M, Tormey D, McGranaghan G, 2021, "A review on turbulent flow over rough surfaces: Fundamentals and theories", *International Journal of Thermofluids* 10:100077.

[15] Menter F, Lechner R, Matyushenko A, 2019, "Best Practice: Generalized k-ω Two-Equation Turbulence Model in ANSYS CFD (GEKO) ", *Technical Report* ANSYS Otterfing.

[16] Ansys® F, 2023, "Ansys Fluent Theory Guide".

[17] Yüksekdağ R, Koçak D, Şentürk U, 2024, "Prediction of heat transfer for a single round jet impingement using the GEKO turbulence model", *International Journal of Heat and Fluid Flow* 109:109538.

[18] Sagot B, Antonini G, Christgen A, Buron F, 2008, "Jet impingement heat transfer on a flat plate at a constant wall temperature", *International Journal of Thermal Sciences* 47:1610–1619.

[19] Menzler JE, Klusmann M, Wulfmeier M, Büschgens D, Pfeifer H, 2023, "Simulation of Gas Jet Impingement Cooling in Continuous Heat Treatment Lines with the ANSYS GEKO Turbulence Model", *HTM Journal of Heat Treatment and Materials* 78:91–104.

[20] Rasheed A, Allauddin U, Ali HM, Uzair M, Verdin PG, Siddiqui YH, 2022, "Heat transfer and fluid flow characteristics investigation using detached ribs in an axisymmetric impinging jet flow", *J Therm Anal Calorim* 147:14517–14537.